UDC 519.85:531.2:539.3:616.77:611.73
Preliminary communication
Received: 28.05.2006.

Modelling and assessment of pneumatic artificial muscle

Li Songbo[(1)], **Jin Jian**[(2)] and **He Qingwei**[(1)]
[(1)]School of Mechanical Engineering, Shanghai Jiaotong University, Shanghai, P.R. CHINA
e-mail: Songbo.Listen@sjtu.edu.cn ; Heqinwei@sjtu.edu.cn
[(2)]Department of Mechanical Automation, Shanghai University, Shanghai, P.R. CHINA

SUMMARY

The pneumatic artificial muscle (PAM) being a new type of actuator is widespread used in engineering field because it possesses the attractive attributes of safe operation, low cost, high output force to volume. It is a prime requirement to establish an effective theoretical model to predict the performance of the PAM as well as other actuators. In this paper a new PAM model is established by employing conservation energy and the Mooney-Rivlin strain energy function for the rubber of PAM. This model is compared with the previous models and the experimental results and it shows that the model truly improves the assessment of forces and contraction that can be achieved by the PAM. However, the significant discrepancy still exists between the theoretical model and the experiment. A number of factors, like friction force, which result in the discrepancy are discussed.

***Key words**: pneumatic artificial muscle, strain energy, Mooney-Rivlin model, testing.*

1. INTRODUCTION

The Pneumatic Artificial Muscle (PAM) (see Figure 1) which was first developed in the 1950's consists of an internal rubber bladder surrounded by a braided mesh shell.

Fig. 1 The geometry of the PAM

The PAM generates longitudinal contraction according to the gas pressure loading on the internal rubber surface. Because of its high force to weight ratio the PAM has a wide range of applications, such as potential projects, vibrators, conveyors, etc, especially in robots.

In this paper we present a model employing hyperelastic theory to describe the inner elastomer bladder and do experiments to test its improvement in prediction of PAM's output force. The previous models mostly ignored the elastic energy of bladder [1-4] and some considered the elastic energy but they did not give the details about the theory and experiment [5]. This paper will give the detailed description of theoretical model and experimental method; lastly, it will provide the contrast between the model predictions and the experimental results.

2. THEORETICAL MODEL DERIVATION

2.1 Basic definition

The elastomer bladder can be described by (T_0, R_0, L_0) in the undeformed state and (T_i, R_i, L_i) in the

deformed state, where the T_0 and T_i stand for the undeformed and deformed thickness, the same as diameter of R_0 and R_i and the length of L_0 and L_i.

The principal strains of the bladder are described according to the cylinder coordinate, i.e., radial strain (λ_1), circumferential strain (λ_2) and axial strain (λ_3). The corresponding principal strains are given by:

$$; \ \lambda_2 = \frac{R_i}{R_0}; \ \lambda_3 = \frac{L_i}{L_0} \tag{1}$$

Note that due to the material incompressibility, these strains are related by:

$$\lambda_1\lambda_2\lambda_3 = 1 \tag{2}$$

In the context of the bladder deformation, this relation is used to calculate the radial strain with the use of the strains λ_2 and λ_3:

$$\lambda_1 = \frac{1}{\lambda_2\lambda_3} = \frac{R_0 L_0}{R_i L_i} \tag{3}$$

2.2 Constitutive equation

Non-linear elastomer materials are classically modeled by hyperelastic constitutive equation [6]. Thus, the material behaviour is represented by a strain energy function, denoted *W*. To isotropic hyperelastic materials, the strain energy function is given by:

$$W = \sum_{i+j=1}^{N} C_{ij}\left(\overline{I_1} - 3\right)^i \left(\overline{I_2} - 3\right)^j + \sum_{i=1}^{N} \frac{1}{D_i}\left(J-1\right)^{2i} \tag{4}$$

In the case of material incompressibility the second term is zero. Then, the Eq. (4) can be simplified as:

$$W = \sum_{i+j=1}^{N} C_{ij}\left(I_1 - 3\right)^i \left(I_2 - 3\right)^j \tag{5}$$

Let *N=1*, we get the linear strain energy function, i.e., Mooney-Rivlin model [6]. This model is one of the simplest rubber models and it will simplify the following discussion. It is defined by two material constants, C_{10} and C_{01}, and the corresponding strain energy function is given by:

$$W = C_{10}\left(I_1 - 3\right) + C_{01}\left(I_2 - 3\right) \tag{6}$$

where I_1 and I_2 which are the reduced strain invariants can be described by the principal strains; then the strain energy function is given as:

$$W = C_{10}\left(\lambda_1^2 + \lambda_2^2 + \lambda_3^2 - 3\right) + \\ + C_{01}\left(\lambda_1^2\lambda_2^2 + \lambda_2^2\lambda_3^2 + \lambda_3^2\lambda_1^2 - 3\right) \tag{7}$$

So, incorporating strain definitions given by Eqs. (1) and (3) into Eq. (7), the strain energy function can be written as:

$$W = C_{10}\frac{4n^2\pi^2 R_0^2 L_0^2}{L_i^2\left(B^2 - L_i^2\right)} + C_{01}\frac{4n^2\pi^2 R_0^2}{B^2 - L_i^2} + C_{10}\frac{B^2 - L_i^2}{4n^2\pi^2 R_0^2} + \\ + C_{01}\frac{L_i^2\left(B^2 - L_i^2\right)}{4n^2\pi^2 R_0^2 L_0^2} + C_{10}\left(\frac{L_i^2}{L_0^2} - 3\right) + C_{01}\left(\frac{L_0^2}{L_i^2} - 3\right) \tag{8}$$

2.3 Model derivation

Using conservation of energy equation, i.e., the input work should equal output work, when PAM's length has a minute change:

$$P'\Delta V = F\Delta L + V_b\Delta W \tag{9}$$

where P' is the relative gas pressure of the bladder, ΔV is the volume change, F is the axial tension, ΔL is the axial displacement, V_b is the elastomer volume, taking directly into account the incompressibility assumption given by Eq. (2), which is a constant, and ΔW is the change of the strain energy function. The Eq. (9) can be given by differential form:

$$F = p'\frac{dV}{dL} - V_b\frac{dW}{dL} \tag{10}$$

where $\frac{dV}{dL}$ can be written as:

$$\frac{dV}{dL} = \frac{-\pi R_0^2}{\sin^2 a_0} \times \left(1 - \frac{3L_i^2\cos^2 a_0}{L_0^2}\right) \tag{11}$$

The relation of *R*, *L*, *B* and a_0 is [4]:

$$\frac{R_i}{R_0} = \frac{\sqrt{1 - \cos^2 a_0 (\frac{L_i}{L_0})^2}}{\sin a_0} \tag{12-a}$$

$$\sin a_0 = \frac{2n\pi R_0}{B} \ ; \cos a_0 = \frac{L_0}{B} \tag{12-b}$$

where a_0 is the angle between the braided thread and the bladder axis, *B* is the total length of the thread. So, using the Eq. (12), Eq. (11) can be expressed simply as:

$$\frac{dV}{dL} = \frac{1}{4\pi n^2} \times \left(3L_i^2 - B^2\right) \tag{13}$$

At the same time, $\frac{dW}{dL}$ can be written as:

$$\frac{dW}{dL} = \frac{8C_{10}n^2\pi^2 R_0^2 L_0^2\left(2L_i^2 - B^2\right)}{\left(B^2 - L_i^2\right)^2 L_i^3} + \frac{8C_{01}n^2\pi^2 R_0^2 L_i^2}{\left(B^2 - L_i^2\right)^2} - \\ - \frac{C_{10}L_i}{2n^2\pi^2 R_0^2} + \frac{C_{01}L_i\left(B^2 - 2L_i^2\right)}{2n^2\pi^2 R_0^2 L_0^2} + \frac{2C_{10}L_i}{L_0^2} - \frac{2C_{01}L_0^2}{L_i^3} \tag{14}$$

Thus, using the Eqs. (13) and (14), the final model can be expressed as:

$$F = \frac{P'}{4\pi n^2} \times \left(3L_i^2 - B^2\right) - V_b \left[\frac{8C_{10}C_0\left(2L_i^2 - B^2\right)}{\left(B^2 - L_i^2\right)^2 L_i^3} + \right.$$
$$+ \frac{8C_{01}C_0L_i^2}{L_0^2\left(B^2 - L_i^2\right)^2} - \frac{C_{10}L_0^2L_i}{C_0} + \frac{C_{01}L_i\left(B^2 - 2L_i^2\right)}{2C_0} +$$
$$\left. + \frac{2C_{10}L_i}{L_0^2} - \frac{2C_{01}L_0^2}{L_i^3} \right] \tag{15}$$

where $C_0 = n^2\pi^2R_0^2L_0^2$ is a constant for specific PAM.

3. RUBBER TENSION EXPERIMENT

To determine the material constants of the Mooney-Rivlin model, C_{10} and C_{01}, the uniaxial tension test is carried out at room temperature using a classical dumbbell-shaped specimen (*20x4x1.65 mm*). After the curve fitting, a comparison of fitted and the experimental (nominal stress-nominal strain) data is plotted in Figure 2.

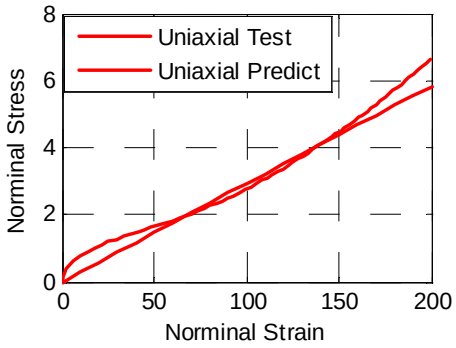

Fig. 2 Fitting curve of Mooney-Rivlin model

From Figure 2, we noticed that the fitted data basically describe the experimental data under the low and median strain. The fitting mechanical constants of rubber is C_{10}=*0.0142 MP*, C_{01}=*0.1008 MP*.

4. PAM EXPERIMENT

4.1 Testing setup

The following testing system which can produce and record the tension, length, and pressure of the PAM is shown in Figure 3.

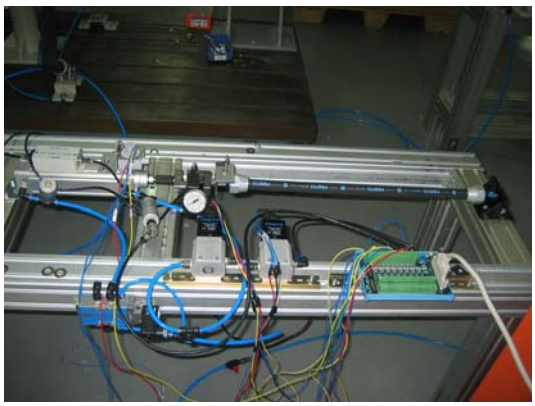

Fig. 3 The PAM testing setup

The hardware includes a personal computer, Advantech integrated board card (PCI 1711), direct current source (*24V*), two FESTO proportional pressure regulators (MPPE-3, *8 bar* max.), tension and compression force sensor (*±5V*), two FESTO pressure sensors (SDE-10-*5V/20mA*), Celesco compact string pot displacement sensor (*50 inches* max.), FESTO air cylinder (DNA-2 1/2", *200 kg* max.), air compressor.

Testing system frame was built with aluminium alloy sections. We made the finite element analysis (FEA) of the frame in order to check whether it has enough stiffness to bear the maximum load of air cylinder. The analysis result shows that the maximal displacement of the frame is less than *0.2 mm*, Figure 4.

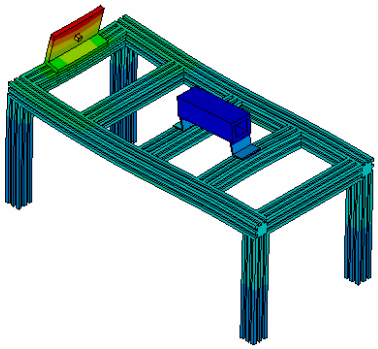

Fig. 4 FEA deformation contour of the testing frame

The software system can control the pressure of the PAM and the air cylinder and save the acquisition data of sensors about the force and the displacement generated by the PAM. The main testing control user interface is shown in Figure 5.

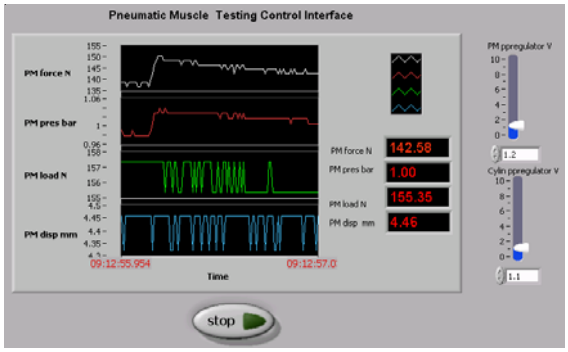

Fig. 5 The user interface of the testing system

4.2 Tested PAMs

In order to verify the predictive force of the model under different conditions, four types of PAM which all belong to FESTO Company were tested in the experiments, the type numbers are MAS-20-500, MAS-10-500, MAS-20-200, MAS-10-200, and all PAM's max. permitted contractions are *25%*. The detailed dimensions are listed in Table 1.

Table 1 The dimensions of the PAMs

Type num	MAS -20-500	MAS -10-500	MAS -20-200	MAS -10-200
L_0 (mm)	500	500	200	200
R_0 (mm)	20	10	20	10
T_0 (mm)	2.8	1.9	2.5	1.7
N (turns)	3.3	2.4	2.1	1.8

4.3 Experimental results

Our focus is to test the output force-contraction of the PAM, therefore, only the constant pressure testing is applied. In the testing the PAM was fixed at one end and free to move subject to the constraint of the air cylinder at the other end. The pressures of air input to PAM and cylinder were controlled by two proportional pressure regulators, a pressure sensor was introduced at the inlet of the tested PAM to make pressure acquisition data recorded on the PC in each instance through the Advantech board card, the same as air cylinder, the only difference was that the software must convert the pressure data to force data using the equation $F_a=P\cdot S_a$ (S_a is the cross-sectional area of the air cylinder), the tensile force collected by the tension and compression force sensor subtracted F_a is the output force of the PAM, the contraction of the PAM was recorded by the displacement sensor.

The experimental results were obtained at activation pressures of *1* to *6 bars*, the testing results of force-contraction profile at varying pressure of *1 bar* to *6 bars* are shown in Figure 6.

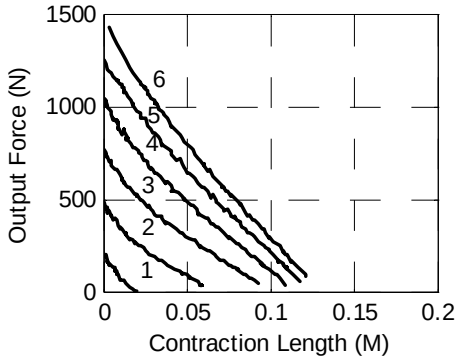

Fig. 6 Force-contraction profile at varying pressure

From Figure 6 it is seen that with the increment of the pressure the linear force-length phenomenon is enhanced, but at *0-10 mm* contraction region the nonlinear force-length relationship is very obvious.

In order to assess the theoretical models, the model of this paper and the model developed by Chou [1] were compared with the experimental results, Figures 7-12.

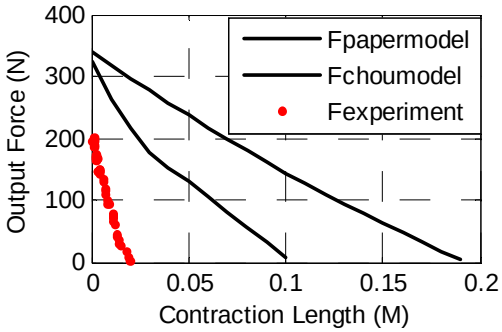

Fig. 7 Force-contraction curve of PAM at 1 bar

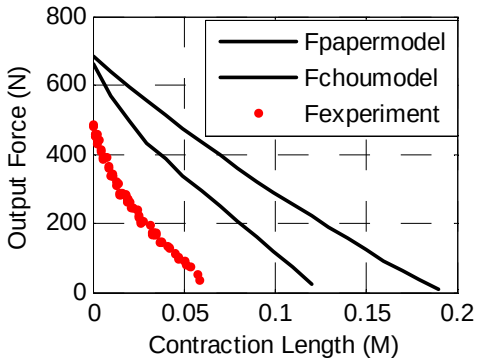

Fig. 8 Force-contraction curve of PAM at 2 bars

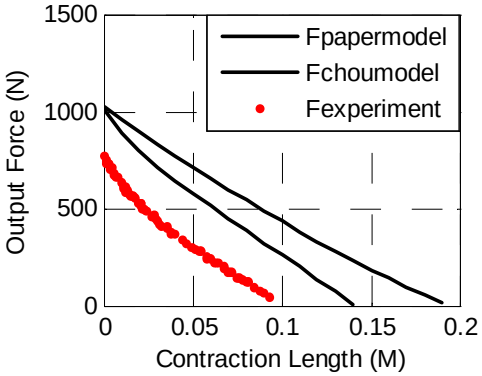

Fig. 9 Force-contraction curve of PAM at 3 bars

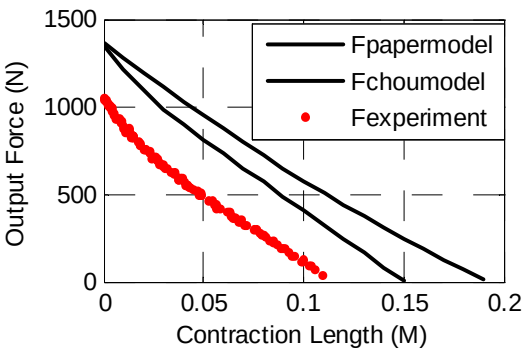

Fig. 10 Force-contraction curve of PAM at 4 bars

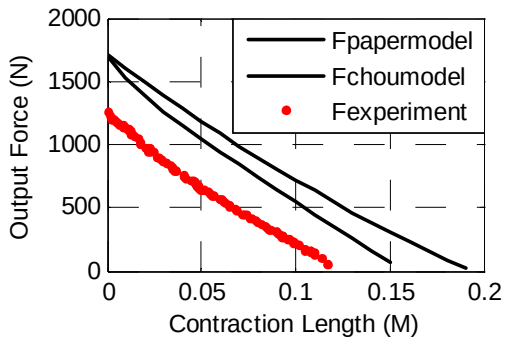

Fig. 11 Force-contraction curve of PAM at 5 bars

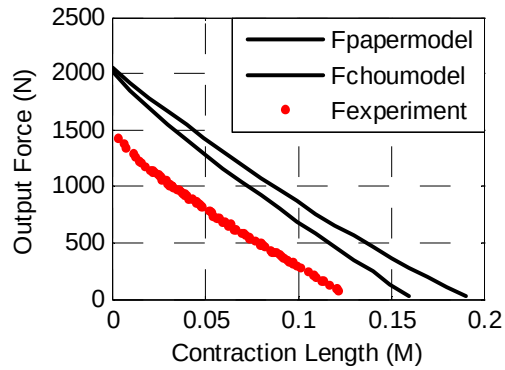

Fig. 12 Force-contraction curve of PAM at 6 bars

A number of conclusions can be drawn from the above figures. Firstly, either our or the model from Chou does not coincide well with the experimental results, the discrepancy produced by neglecting the friction, pressure loss, the tip-effects of the PAM's ends (a violation of the theoretical right circular cylinder assumption) and other factors is significant. Secondly, the new model is more accurate than the model from Chou, especially at mid to high contraction. Lastly, at the low pressure (Figures 7 and 8) the theoretical results including the magnitude and shape of the curve cannot correspond with the testing results; but at the high pressure (Figures 11 and 12) the theoretical model curve shapes basically correspond well with the testing curves. In other words, due to ignoring the friction force and other factors, the approximation of theoretical model to experiment is only the approximation of curve shape unless the output force is large enough to ignore the existence of the friction.

5. CONCLUSIONS AND RECOMMENDATIONS

In this paper the theoretical PAM model which considers the elastic energy described by incompressible Mooney-Rivlin equation was derived and assessed. The more reasonable model would be found very useful to describe the static displacement and force performance of PAM based systems.

In the present paper only the elastic energy factor was considered and the significant effects of the friction and other energy loss can be clearly found in Figures 7 upto 12. In order to perfect the PAM model, using the sound approach to account for effect of the friction is the main aim of the further work.

ACKNOWLEDGEMENTS

The authors would like to express their gratitude to Dan Wenjiao and to Zhang Guoxing, Engineering Department Manager of the FESTO China in Shanghai, for the constant support of this research.

6. REFERENCES

[1] C.P. Chou and B. Hannaford, Measurement and modeling of McKibben pneumatic artificial muscles, *IEEE Transactions on Robotics and Automation*, Vol. 12, No. 1, pp. 90-102, 1996.

[2] C.P. Chou and B. Hannaford, Static and dynamic characteristics of McKibben pneumatic artificial muscles, Proceedings of the IEEE International Conference on Robotics and Automation, San Diego, IEEE, Vol. 1, pp. 281-286, 1994.

[3] N. Tsagarakis and D.G. Caldwell, Improved modeling and assessment of pneumatic muscle actuators, Proceedings of the ICRA 2000 IEEE International Conference on Robotics and Automation, San Francisco, IEEE, Vol. 4, pp. 3641-3646, 2000.

[4] B. Tondu and P. Lopez, Modeling and control of McKibben artificial muscle robot actuators, *IEEE Control Systems Magazine*, Vol. 20, No. 2, pp. 15-38, 2000.

[5] G.K. Klute and B. Hannaford, Accounting for elastic energy storage in McKibben artificial muscle actuators, *ASME Journal of Dynamic Systems, Measurements and Control*, Vol. 122, pp. 386-388, 2000.

[6] L.R.G. Treloar, *The Physics of Rubber Elasticity*, Clarendon Press, Oxford, 1975.

[7] E. Verron and G. Marckmann, Numerical analysis of rubber balloons, *Thin-Walled Structures*, Vol. 41, pp. 731-746, 2003.

MODELIRANJE I PROCJENA PNEUMATSKOG UMJETNOG MIŠIĆA

SAŽETAK

Pneumatski umjetni mišić (PAM), kao novi tip, uvelike se koristi u tehnici budući da ima atraktivna svojstva sigurnog rada, malog troška i veliki izvor snage u odnosu na volumen. Prvi zahtjev je, kao i kod drugih pobuđivača, napraviti efektivni teorijski model kojim bi se predvidio rad PAM-a. Ovaj rad prikazuje novi PAM model koristeći se održanom energijom i funkcijom Mooney-Rivling-ove energije deformiranja za gumeni materijal PAM-a. Ovaj PAM model se uspoređuje s prethodnim modelima i rezultatima eksperimenata te se pokazuje da ovaj PAM model uistinu poboljšava procjenu sila i kontrakcija. Ipak, postoji značajan nesklad između teorijskog modela i eksperimenata. Raspravlja se o brojnim čimbenicima, poput sile trenja, koji ukazuju na taj nesklad.

***Ključne riječi**: pneumatski umjetni mišić, energija deformiranja, Mooney-Rivlin-ov model, ispitivanje.*